

# Neutron Production by Cosmic-Ray Muons in Various Materials

K. V. Manukovsky,<sup>1,2</sup> O. G. Ryazhskaya,<sup>1</sup> N. M. Sobolevsky,<sup>1,3</sup> and A. V. Yudin<sup>1,2,\*</sup>

<sup>1</sup>*Institute for Nuclear Research, Russian Academy of Sciences,  
pr. Shestidesyatiletija Oktyabrya 7a, Moscow, 117312 Russia*

<sup>2</sup>*Institute for Theoretical and Experimental Physics,  
Bolshaya Cheremushkinskaya 25, Moscow, 117218 Russia*

<sup>3</sup>*Moscow Institute of Physics and Technology (State University),  
Institutskii Lane 9, Dolgoprudnyi, Moscow Region, 141700 Russia*

The results obtained by studying the background of neutrons produced by cosmic-ray muons in underground experimental facilities intended for rare-event searches and in surrounding rock are presented. The types of this rock may include granite, sedimentary rock, gypsum, and rock salt. Neutron production and transfer were simulated using the Geant4 and SHIELD transport codes. These codes were tuned via a comparison of the results of calculations with experimental data, in particular, with data of the Artemovsk research station of the Institute for Nuclear Research (INR, Moscow, Russia) as well as via an intercomparison of results of calculations with the Geant4 and SHIELD codes. It turns out that the atomic-number dependence of the production and yield of neutrons has an irregular character and does not allow a description in terms of a universal function of the atomic number. The parameters of this dependence are different for two groups of nuclei: nuclei consisting of alpha particles and all of the remaining nuclei. Moreover, there are manifest exceptions from a power-law dependence, for example, argon. This may entail important consequences both for the existing underground experimental facilities and for those under construction. Investigation of cosmic-ray-induced neutron production in various materials is of paramount importance for the interpretation of experiments conducted at large depths under the Earth's surface.

Keywords: cosmic rays, underground experiments, neutrons, muons

---

\* yudin@itep.ru

## INTRODUCTION

Searches for rare events, including neutrino signals from collapsing stars, neutrino oscillations, proton decay, and traces of dark-matter particles, are being performed at underground experimental facilities. The problem of the background generated by natural rock radioactivity and by cosmic-ray muons is a key problem in such experiment. High-energy muons penetrate easily through rock to large depths, reaching underground facilities and producing neutrons in direct interactions with nuclei and, starting from a depth of several hundred meters, in hadron and electromagnetic showers. It is noteworthy that neutron production may proceed both in the facility itself and in surrounding structures, shielding materials, and rock. A background produced in rock is especially hazardous since this may imitate rare events: high-energy neutrons produced in such processes and moderated in rock may go far away from the track of the parent muon, becoming “isolated” [1, 2]. Coincidence schemes are then unable to remove captures of such neutrons in the active zone of the facility, and this may distort strongly experimental results.

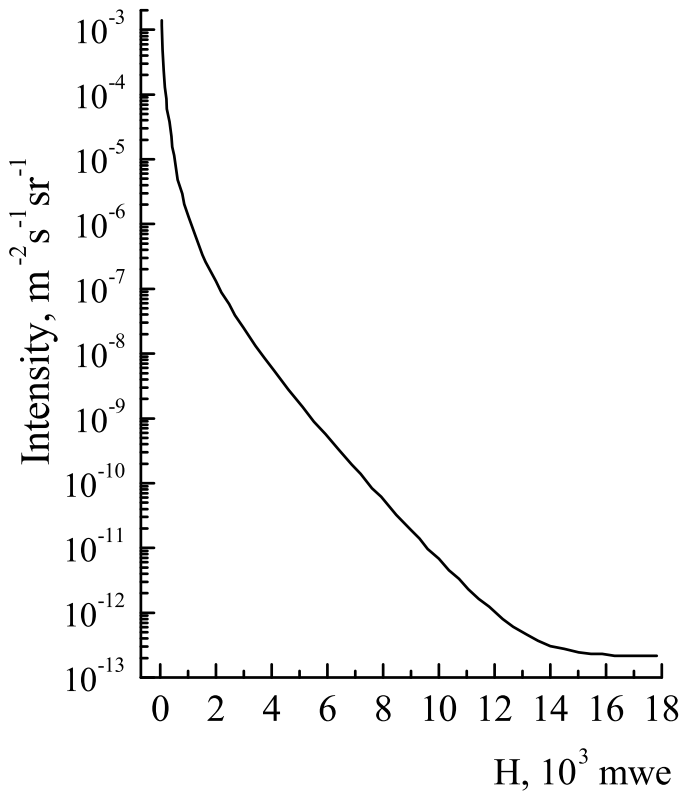


FIG. 1. Intensity of muon flux as a function of depth.

The originally prevalent opinion was that, as disposition of experiments becomes deeper, the contribution of cosmic-ray muons to the formation of the background should decrease substantially in proportion to the reduction of the muon-flux intensity (see Fig. 1), but this proved to be untrue. The decrease in the muon-flux intensity is accompanied by the increase in the mean energy of muons involved. This increase terminates only at a depth of about 10 kmwe at the mean muon energy of about 430 GeV. The important role of processes involving the production of nuclear-active particles in hadron showers formed in muon inter-

actions with nuclei of surrounding matter and the need for taking such processes into account were first highlighted in [3]. The  $\mu + A \rightarrow \mu + n\pi + \chi$  reaction induced by deep-inelastic interactions of muons  $\mu$  with rock nuclei  $A$  leads to the breakup of these nuclei to fragments  $\chi$  and to multiparticle production of pions  $\pi$ , and this gives rise to a further development of the nuclear cascade. At the depth of 4000 mwe, for example, the disregard of this process leads to a neutron-background intensity underestimated by a factor of 2.5 [4]. At large depths, electromagnetic showers are yet another important source of neutrons.

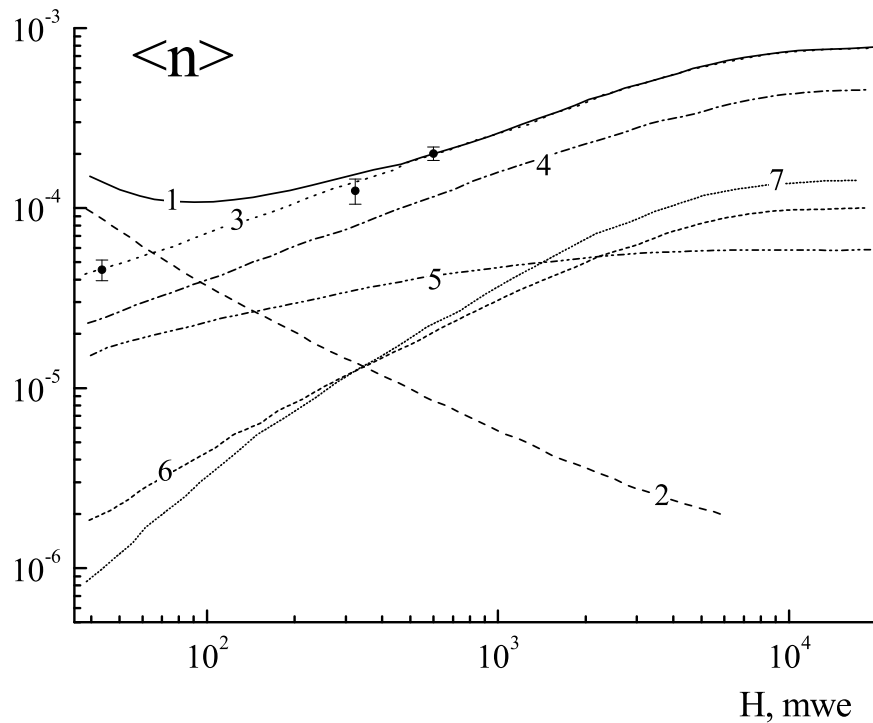


FIG. 2. Number of product neutrons in  $1 \text{ g cm}^{-2}$  of rock per muon as a function of depth: (curves) contributions of various processes (see main of the text) and (points) results of the experiments under discussion.

The contributions of various processes to neutron production per muon are shown in Fig. 2 versus depth measured from the boundary of the Earth's atmosphere. In this figure, curve 1 represents the total number of neutrons produced in all processes. At moderately small depths (up to about 80 mwe),  $\mu^-$  capture (curve 2 in Fig. 2) is a dominant source of neutrons. At large depths, neutrons are predominantly produced in nuclear showers (curve 4) initiated by pions originating from the deep-inelastic interaction of muons with surrounding-matter nuclei and from electromagnetic showers generated by delta electrons, bremsstrahlung

photons, and electron–positron pairs (curves 5, 6, and 7, respectively). Curve 3 stands for the total number of neutrons produced in all processes with the exception of the  $\mu^-$  – capture process. Figure 2 shows that, at depths larger than 1000 mwe, the contribution of nuclear showers to neutron production exceeds the contribution of electromagnetic showers by a factor of 1.5.

The points with error bars in Fig. 2 represent data from the experiments discussed below and performed at the rock thicknesses of 25, 316 and 570 mwe and the mean muon energies of 16.7, 86, and 125 GeV, respectively.

### DEBUGGING THE GEANT4 CODE PACKAGE

In the calculations described below, the results were obtained by using the Geant4 code package in version 9.4 (patch 2) [5]. This code package permits detailed Monte Carlo calculations of particle propagation through matter, possesses means necessary for visualizing objects of complicated geometric shapes, and incorporates a broad set of theoretical models describing particle interactions with matter. Particular attention was given to the choice of physical models that are necessary for accurately describing neutron production and propagation. The set of neutrons originating from the interaction of cosmic–ray muons with matter nuclei can be broken down into four groups [6]. Primary neutron originate directly muon–nucleus interaction (upon the capture of a negatively charged muon and muon spallation), while secondary neutrons arise in nuclear and electromagnetic showers. At small depths of up to 100 mwe, neutrons produced upon muon capture are dominant, while, at large depths (a few thousand mwe units) hadron and electromagnetic showers are the main source of neutrons.

Thus, many mechanisms are involved in the neutron-production process. In view of this, it is necessary to employ a broad set of physical models that describe particle–interaction processes in various energy ranges lying between a few eV units and several hundred GeV units. The Geant4 code package incorporates several standard versions of tuning of physical models. In our calculations, we employ our own set of models, relying on the analysis reported in [7].

Let us mention briefly some important special features of our approach. Final states of nuclei in photonuclear interaction with a muon are described on the basis of the chiral–

phase-space (CHIPS) model for photon energies below 3 GeV; at higher energies, use is made of the quark-gluon string (QGS) model. We apply the QGS model in describing nuclear interactions at high energies (above 12 GeV) and the binary-intranuclear-cascade (BiC) model at low energies (below 6 GeV for neutrons and protons and below 1.5 GeV for pions) and employ the low-energy parametrized (LEP) model in the case of reactions in the range of intermediate energies. One can observe manifestations of matching of the different physical models in Fig. 6 below: the calculated value of the specific neutron yield in a lead target is 15% lower than experimental data at a proton energy of about 10 GeV (see also the relevant discussion below). In order to remove the excitation of the resulting nucleus, we used models that take into account evaporation, fission, Fermi breakup, and multifragmentation (in the case of highly excited nuclei) processes. A model based on the tables of experimentally measured cross sections from the ENDF/B-VI database is used to describe the transport of low-energy neutrons (whose energy does not exceed 20 MeV) with allowance for elastic and inelastic scattering, capture, and nuclear fission.

All of the results of our simulation that are presented below were obtained on the basis of the same set of physical models.

## COMPARISON WITH EXPERIMENTAL DATA

In order to control the accuracy of our calculations and the debugging of the Geant4 code package, we perform a series of test calculations and comparisons of calculated data with known experimental results.

As a starting point, we address the simple case where one irradiates a cylindrical lead target of specific size with protons of various energy (Fig. 3) and perform a simulation of the neutron yield from it for this case known from the literature. Experimental data and the results of our calculations with the aid of the Geant4 code package and calculations of other authors from the review article of Barashenkov [8] are given in Table I, where good agreement between the calculated and experimental data can be seen.

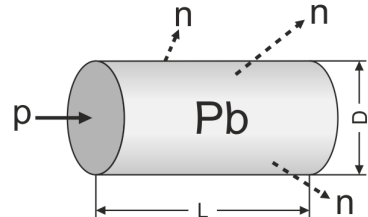


FIG. 3. Cylindrical lead target of diameter  $D$  and length  $L$

TABLE I. Mean number of neutrons escaping from a cylindrical target of diameter  $D$  per primary proton of energy  $E_p$  (the target length is  $L = 61$  cm)

$D$ , cm	$E_p$ , GeV	Number of neutrons		
		calculations [8]	experimental data [8]	Geant4-based calculations
10.2	0.47	$7.8 \pm 0.3$	$8 \pm 0.4$	6.97
			$6.4 \pm 0.3$	
10.2	0.96	$17.8 \pm 0.6$	$16.6 \pm 0.8$	16.65
			$16.8 \pm 0.5$	
			17.7	
10.2	1.47	$25.1 \pm 0.1$	$26.4 \pm 1.3$	25.1
			$27.5 \pm 0.6$	
			29.4	
20.4	0.47	$8.1 \pm 0.3$	$8.7 \pm 0.4$	7.92
		9.2		
20.4	0.96	$21.7 \pm 0.8$	$20.3 \pm 1.1$	20.36
		22.2		
20.4	1.47	$31.5 \pm 1.2$	$31.5 \pm 1.6$	31.84

We also perform a test simulation of the propagation of cosmic-ray muons for various experimental facilities of the Artemovsk research station of the Institute for Nuclear Research (INR, Moscow, Russia) [1, 9, 10] that involve detectors based on a liquid scintillator: specifically, in a gypsum mine at a depth of 25 mwe [10] and in rock-salt mines at the depths of 316 and 570 mwe [10, 11] (see also Fig. 2). The layout of the first facility for experiments at the depths of 25 and 316 mwe is shown in Fig. 4. The surrounding rock is represented by two plane layers 5 m thick above and below the facility, as can be seen in Fig. 4 (volumes T and B, respectively). Fixed energy muons are assumed to travel vertically downward at the facility center. Of the three rectangular scintillation volumes (1–3), only volume 2 serves for data acquisition, while the remaining two accomplish event selection. Moreover, the central volume (2) is surrounded by paraffin (P). For a muon effect to be included in the accumulated data sample, the respective muon should deposit at least 55 MeV in each of

volumes 1 and 3 and not less than 110 MeV in the detecting volume (2).

The layout of the facility for experiments at the depth of 570 mwe is shown in Fig. 5. Here, the detecting scintillation volume is a cylindrical (1), and the event-selection criterion requires that a muon deposit not less than 1 GeV in this volume.

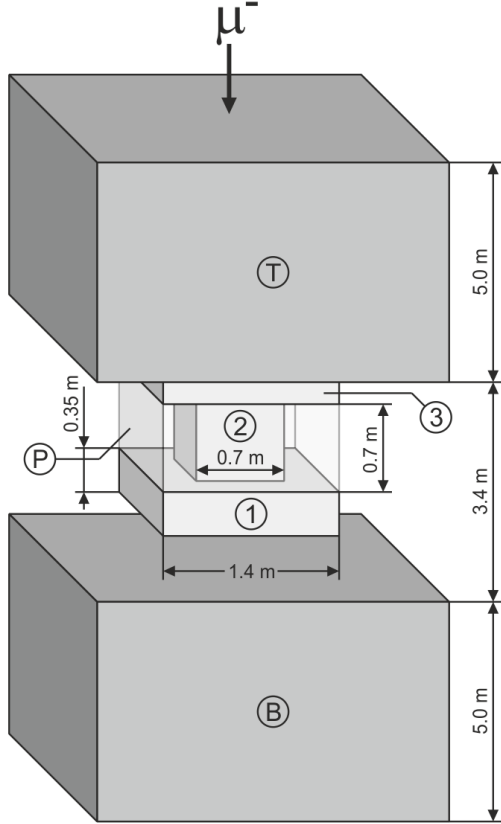


FIG. 4. Layout of the setup for experiments at the depths of 25 and 316 mwe. Volumes T and B simulate surrounding rock, while volumes 1–3 represent the scintillator used; P stands for surrounding paraffin.

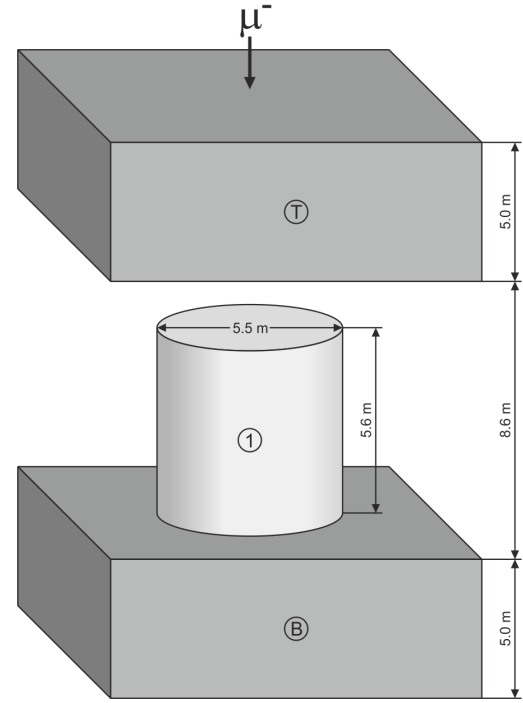


FIG. 5. Layout of the setup for experiments at the depth of 570 mwe. Volumes T and B simulate surrounding rock, while volume 1 stands for the scintillator used.

Table 2 gives experimental and calculated values of the neutron-production yield per 1 g/cm<sup>2</sup>,  $Y_n \equiv N_n / (\rho N_\mu l_\mu)$ , over the volume of the detecting scintillation counter. Here,  $N_n$  is the number of product neutrons,  $N_\mu$  is the total number of muons that traversed the facility and which passed selection criteria, and  $l_\mu$  is muon range in matter of density  $\rho$ . From Table 2, one can see that the calculated and experimental data are very close to each other. In

order to assess the effect of the rock surrounding the experimental facility on the number of product neutrons, we perform a series of calculations, replacing the substance surrounding the detector by various materials, such as rock salt, scintillator, or gypsum. Table 2 shows that this effect is rather weak and becomes noticeable at the minimum value of the muon energy. The number of neutrons captured in the volume of the same scintillation counter exhibits a similar behavior. Thus, the presence of rock has but a slight effect on the total of product neutrons detected by the counter.

TABLE II. Comparison of the experimental and calculated values of the neutron-production yield  $Y_n$  at various depths for various materials surrounding scintillation counters (in  $n/\mu/(g/cm^2)$  units). LS denote a liquid scintillator.

Depth, mwe	Experiment		Calculation			
	$E_\mu$ , GeV	$Y_n$	$E_\mu$ , GeV	$Y_n$		
				rock salt	LS	gypsum
25	$16.5 \pm 8.1$	$0.36 \pm 0.03$ [12]	16.8	0.388	0.55	0.392
	$16.7 \pm 8.2$	$0.47 \pm 0.05$ [10]				
316	$86 \pm 18$	$1.2 \pm 0.12$ [10]	86	1.2	1.26	1.28
570	$125 \pm 22$	$2.04 \pm 0.24$ [11]	125	1.71	1.64	—

## COMPARISON OF THE RESULTS BASED ON THE APPLICATION OF THE SHIELD AND GEANT4 CODES

In order to calibrate Geant4 debugging, we compare the results of our calculations for a test problem with the results reported in [13] and obtained by using the SHIELD transport code [14], which proved to be successful in various applications. As a test problem, we once again consider the problem of the neutron yield from a lead target irradiated with a proton beam whose energy varies over a broad range. The target dimensions are  $L = 60$  cm in length and  $D = 20$  cm in diameter. The results are shown in Fig. 6, where the quantity  $N_n/(N_p E_p)$  is plotted versus energy. Here,  $N_n$  is the number of neutrons that escaped from the target volume and  $N_p$  and  $E_p$  are, respectively, the number of protons and their energy in GeV units. The open symbols with error bars stand for experimental data from various sources. The solid and dashed curves represent the results based the application of, respectively, the

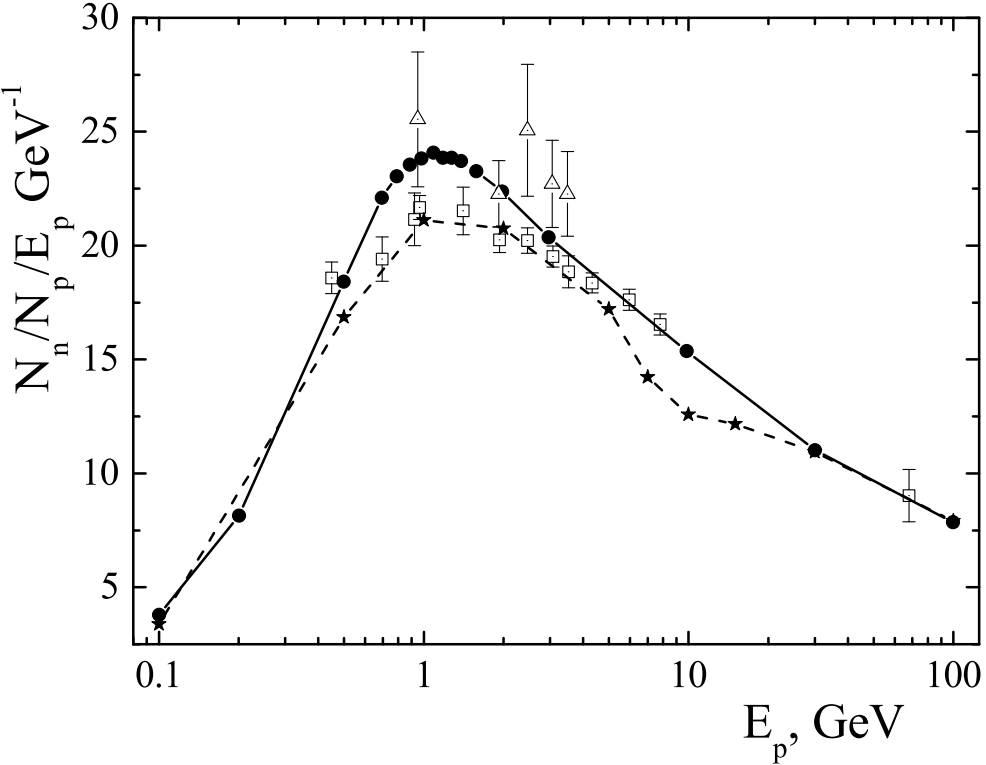


FIG. 6. Specific yield of neutrons from a cylindrical lead target as a function of proton energy. The displayed points stand for experimental data. The solid and dashed curves represent the results of the calculations performed by using the SHIELD and Geant4 codes, respectively.

SHIELD and Geant4 codes. The uppermost group of five experimental points represented by open triangles is worthy of special note. These are data from [15], and a point from the lowest group (boxes) corresponds to each point in the uppermost group. They were obtained within the same experiment but by different methods. The reason behind this difference is not clear; therefore, there are doubts about the reliability of these five points. With allowance for the experimental uncertainties, the two transport codes yield anyway mutually consistent results, which agree with experimental data. As was mentioned above, the discrepancy with experimental data in Geant4-based calculations around  $E_p \sim 10$  GeV is due to the absence of an adequate model for describing interactions in the energy range between the ranges of applicability of the BiC and QGS theoretical models. Among all possibilities that are available within Geant4 at the present time and which we considered here, the use of the LEP model provides results that are the closest to experimental data in the energy range between 1.5 and 12 GeV, but which are by no means precise.

## NEUTRON PRODUCTION BY MUONS

### Dependence on the Atomic Weight

In order to determine the dependence of the number of product neutrons on the atomic weight of the material being considered, we perform a numerical simulation of muon propagation for muons of various energy through a target having a simple geometric shape and featuring a uniform density distribution, the size of the target being infinite in the direction orthogonal to the muon velocity (see Fig. 7).

For each material, the total target thickness was chosen to be equivalent to  $2000 \text{ g cm}^{-2}$ , which corresponds to the mean muon energy loss of about 5% (for muons of energy 100 GeV). The results of the calculation for muons of energy 100 and 280 GeV are given in Figs. 8 and 9, respectively. They show the neutron production yield  $Y_n$  [neutrons/muon/( $\text{g cm}^{-2}$ )] as a function of the mean atomic weight of the target material. It should be noted that the data presented here were obtained upon the event selection on the basis of the spectrum of muon energy depositions: events in which the muon energy deposition in the target exceeded half of the most probable energy deposition were selected for a comparison with experimental data. A detailed analysis reveals that the selection in question has but a slight effect on the production yield and does not lead to qualitative changes in the character of the resulting dependencies.

The calculated values of the number of product neutrons can be broken down into three groups markedly different in the target chemical composition: those for targets free from alpha-particle nuclei (for example, Fe or NaCl); those for targets from purely alpha-particle nuclei (C, Ca, and so on); and those for targets from materials of mixed composition (such as the rock of the Gran Sasso underground laboratory), in which case the fraction of alpha-particle nuclei is indicated in the figure. In the first group, the neutron production yield  $Y_n(A)$  is well approximated by a dependence of the form  $Y_n(A) \propto A^k$ , where  $k \approx 0.82$  for  $E_\mu = 100 \text{ GeV}$  and  $k \approx 0.89$  for  $E_\mu = 280 \text{ GeV}$  (upper curves in Figs. 8 and 9). For

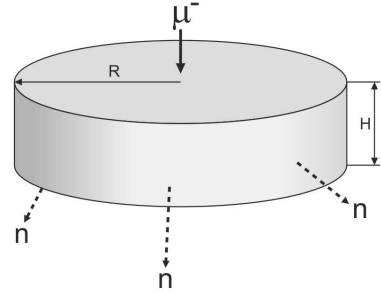


FIG. 7. Scheme of a numerical experiment for determining the dependence of the number of product neutrons on the atomic weight of materials.

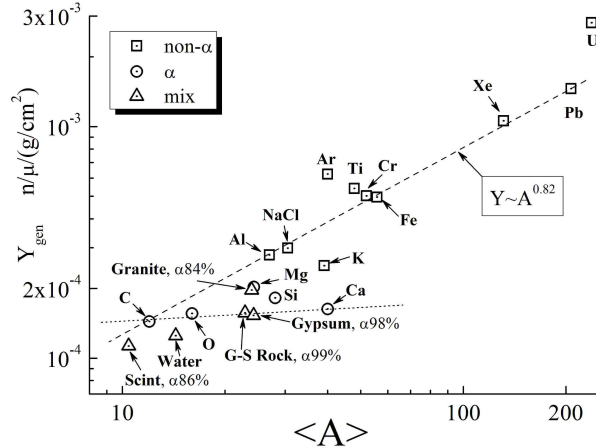


FIG. 8. Neutron-production yield as a function of the atomic weight of matter for muons of energy 100 GeV.

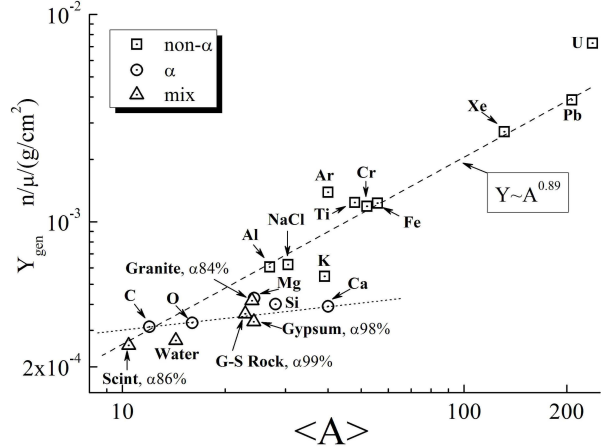


FIG. 9. As in Fig. 8, but for the muon energy of 280 GeV. G-S denotes the rock of the Gran Sasso underground laboratory.

alpha-particle nuclei, the atomic-weight dependence of the number of product neutrons is weak (lower curves). Finally, the dependence for materials of mixed composition exhibits an intermediate behavior between the preceding two cases, the relative positions of the curves correlating substantially with the fraction of alpha-particle nuclei in the chemical composition of the target. Nevertheless, some chemical elements (for example, potassium and uranium) do not fit satisfactorily in this pattern.

In addition to the number of product neutrons, the calculations made it possible to determine the number of neutrons that escaped from the target. The results for muons of energy 100 and 280 GeV are shown in Figs. 10 and 11. The neutron yield depends not only on the atomic weight but also on many other extra factors (such as the target size and shape and the parameters of the neutrons-transfer process) and therefore does not follow any simple dependence [16]. It follows that only via a numerical simulation can one precisely estimate the neutron background generated by cosmic-ray muons in modern underground detectors of complicated design.

### Dependence on the Muon Energy

The energy dependence of the neutron-production yield is frequently represented in the power-law form  $Y_n \sim E_\mu^n$ , where the exponent  $n$  is smaller than or on the order of unity.

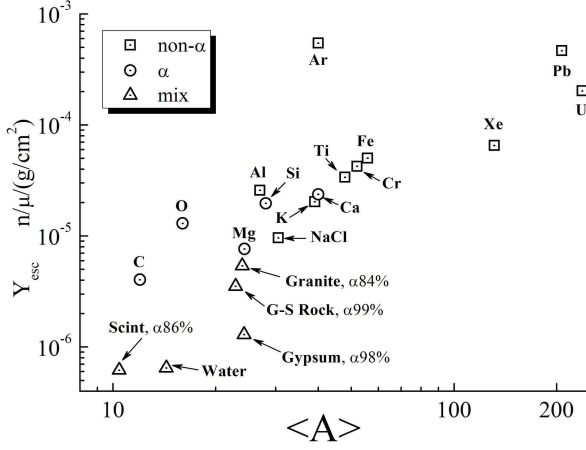


FIG. 10. Neutron yield as a function of the atomic weight of materials for muons of energy 100 GeV.

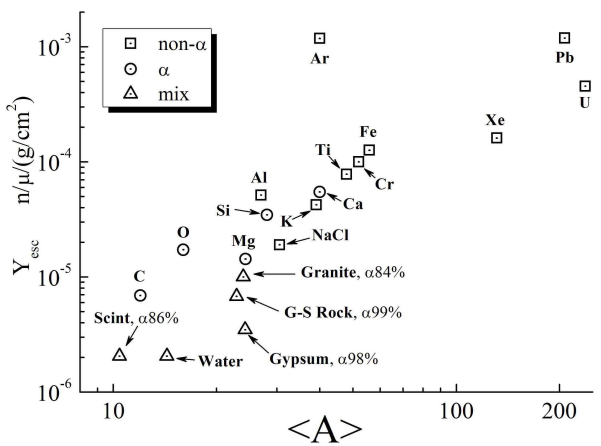


FIG. 11. As in Fig. 10, but for the muon energy of 280 GeV.

Figure 12 shows the values of the effective exponent  $n_{\text{eff}}$  that were obtained from a comparison of the production yields at the muon-energy values of 100 and 280 GeV for the same materials as in the preceding figures. The majority of these values fall within a rather narrow range, the average value being 0.75. Alpha-particle nuclei show a moderate muon-energy dependence; for other materials, the exponent is somewhat higher, and there is a trend toward an increase in  $n_{\text{eff}}$  with increasing  $A$ . Uranium and lead have a maximum value of  $n_{\text{eff}} \lesssim 1$ .

### A. Case of Argon

Argon and calcium attract particular attention, since these species, which have very close atomic weights, differ strongly (several fold) in the number of product neutrons. In order to study this effect, we perform a calculation on the basis of the SHIELD transport code for the problem of a cylindrical target (its radius and length are  $R = 1.5$  m and  $L = 3$  m, respectively) irradiated along the axis with a beam of negatively charged pions with energies of 1, 10, and 100 GeV (see Fig. 13)

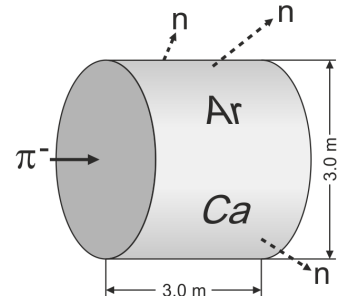


FIG. 13. Scheme of a numerical experiment that employs the SHIELD transport code.

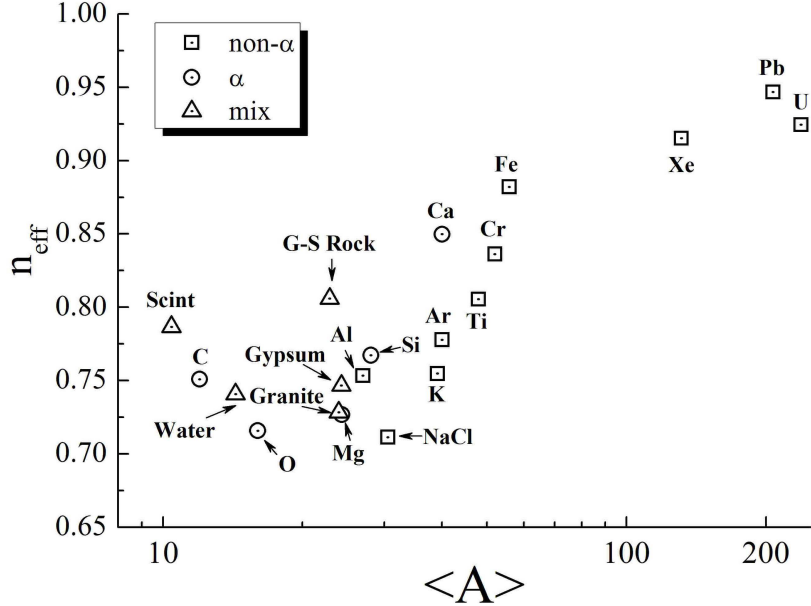


FIG. 12. Effective exponent  $n_{\text{eff}}$  in the muon–energy dependence of the neutron–production yield,  $Y_{\text{n}} \sim E_{\mu}^{n_{\text{eff}}}$ .

Liquid argon ( $\rho = 1.65 \text{ g cm}^{-3}$ ) or calcium ( $\rho = 1.55 \text{ g cm}^{-3}$ ) serve as a target material. The neutron production and neutron yield from the target are calculated. In the case being considered, the former is the number of neutrons characterized by energies below 14.5 MeV and produced within the target in hadron-induced nuclear reactions (they include cascade neutrons of energy above 14.5 MeV). The latter is the number of neutrons whose energy is below 14.5 MeV and which go beyond the target boundary. The results are presented in Table III.

TABLE III. Comparison of the production and yield of neutrons for a cylindrical target ( $R = 1.5 \text{ m}$  and  $L = 3 \text{ m}$ ) exposed to pions of various energy (liquid argon or calcium serves as a target material)

$E_{\pi},$ GeV	Ar		Ca	
	production	yield	production	yield
1	16.7	17.1	7.47	4.69
10	77.0	78.8	33.6	20.7
100	381	390	161	99.1

The reasons behind the large distinction between the results for  $^{40}\text{Ar}$  and  $^{40}\text{Ca}$  are the following. First, the neutron multiplicity is higher in hadron–nucleus reactions on argon. Indeed, the energies of separation of a single neutron and a neutron pair from the  $^{40}\text{Ar}$  nucleus are 9.87 and 16.5 MeV, respectively, but, for  $^{40}\text{Ca}$ , the respective energies are 15.6 and 29.0 MeV [17].

The second reason is that the neutron cross sections at energies below 14.5 MeV are markedly different for these two nuclear species. Figure 14 shows the cross sections for reactions in calcium and argon versus the neutron energy  $E_n$ . The figures on the lines mark the cross sections for (1) capture, (2) inelastic scattering, (3) elastic scattering, and (4) ( $n, 2n$ ) reactions. The thick line represents the total cross. In argon, the ( $n, 2n$ ) reaction proceeds, but there is no such reaction in calcium. Moreover, this figure shows that the total cross section for neutrons of energy below about 0.1 MeV in argon is three to four times smaller than its counterpart for calcium. Accordingly, the neutron ranges in argon are three to four times longer than those in calcium, and this facilitates neutron escape from the target volume.

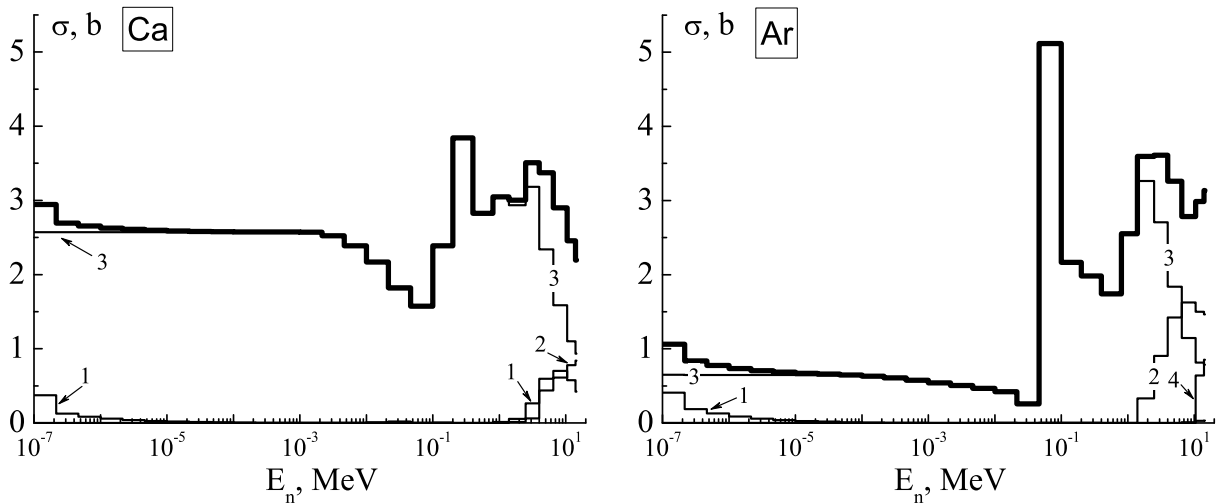


FIG. 14. Comparison of the energy dependences of the group cross sections from [18] for neutron reactions in calcium and argon. The notation used is explained in the main body of the text.

## CONCLUSIONS

The importance of correctly taking into account the background in experiments devoted to searches for rare events is worth emphasizing in conclusion. The effect of the irremovable (in principle) background of neutrons produced by cosmic-ray muons under the Earth's surface is treatable properly only if we are able to calculate it correctly with allowance for all special features of the experimental setup being considered, the surrounding shielding elements, and rock. The above example of the comparison of calcium and argon shows that the use of oversimplified model concepts of neutron-production processes in various materials may lead to a significant (several fold) deviations from true result. The foregoing is all the more true since liquid argon, which is a strong source of neutrons, is an indispensable ingredient of many experiments conducted at the present time (see, for example, [19]). Thus, only a thorough understanding of processes involving neutron production by cosmic rays in various materials would make it possible to interpret correctly the results of experiments performed at large depths under the Earth's surface.

## ACKNOWLEDGMENTS

This work was supported in part by the Russian Foundation for Basic Research (project no. 15–02–01056\_а) and was funded by a grant (no. 3110.2014.2) for support of leading scientific schools. The financial support within the program of basic investigations of Presidium of Russian Academy of Sciences Fundamental Properties of Matter and Astrophysics is also gratefully acknowledged.

## REFERENCES

---

- [1] R. I. Enikeev et al., Sov. J. Nucl. Phys. **46**, 883 (1987).
- [2] N. Yu. Agafonova et al., Bull. Russ. Acad. Sci.: Phys. **73**, 628 (2009).
- [3] O. Ryazhskaya and G. Zatsepin, in *Proceedings of the 9th International Conference on Cosmic Rays*, ICCR, London, UK, **2**, 987 (1965).

- [4] O. G. Ryazhskaya, Phys. Usp. **56**, 296 (2013).
- [5] V. N. Ivanchenko (for Greant4 Collab.), Nucl. Instrum. Methods Phys. Res. A **502**, 2, 666 (2003).
- [6] A. S. Malgin and O. G. Ryazhskaya, Phys. At. Nucl. **71**, 1769 (2008).
- [7] A. Lindote et al., Astropart. Phys. **31**, 366 (2009).
- [8] V. S. Barashenkov, Sov. J. Part. Nucl. **9**, 315 (1978).
- [9] L. B. Bezrukov et al., Acta Phys. Acad. Sci. Hung. **29** (Suppl. 4), 285 (1970).
- [10] L. B. Bezrukov et al., Sov. J. Nucl. Phys. **17**, 51 (1973).
- [11] O. G. Ryazhskaya, Doctoral (Phys. Math.) Dissertation (Inst. Nucl. Res. Russ. Acad. Sci., Moscow, 1986).
- [12] F. Boehm et al., Phys. Rev. D **62** 072002 (2000).
- [13] A. V. Dementyev, N. M. Sobolevsky, and Yu. Ya. Stavissky, Nucl. Instrum. Methods Phys. Res. A **374**, 70 (1996).
- [14] <http://www.inr.ru/shield/>
- [15] R. G. Vassil'kov and V. I. Yurevich, in Proceedings of the 11th Meeting of the International Collaboration on Advanced Neutron Sources ICANS-11, KEK, Tsukuba, Japan, **1**, 340 (1990); KEK Report No. 90-25 (1991).
- [16] N. Yu. Agafonova and A. S. Malgin, Phys. Rev. D **87**, 113013 (2013).
- [17] V. A. Kravtsov, Atomic Masses and Nuclear Binding Energies (Atomizdat, Moscow, 1974) [in Russian].
- [18] L. P. Abagyan, N. O. Bazazyants, M. N. Nikolaev, and A. M. Tsibulya, *Neutron Group Constants for Reactors and Shielding Calculations, The Handbook* (Energoizdat, Moscow, 1981) [in Russian].
- [19] *Proceedings of the 14th International Workshop on Neutrino Telescopes*, Venice, Italy, (2011).